2017 IEEE International Conference on Robotics and Automation (ICRA)
Singapore, May 29 - June 3, 2017

Path Following Control of Skid-Steered Wheeled Mobile Robots at Higher Speeds on Different Terrain Types

Goran Huskić, Sebastian Buck and Andreas Zell

***Abstract*— A new nonlinear control law for path following with skid-steered mobile robots is proposed. A terrain dependent kinematic model is utilized in path coordinates, and the kinematic parameters are experimentally evaluated. A kinematic path following control is developed using the Lyapunov approach. A separate linear velocity control is then proposed, taking reachable curvatures and actuator saturation into account. The proposed approach is experimentally evaluated in different terrain scenarios, and compared with two other state-of-the-art algorithms. The skid-steered vehicle used for the experiments is the Robotnik Summit XL, a well known commercial mobile robot.**

I. INTRODUCTION

Path following control is one of the basic tasks for mobile robots, which becomes more challenging at higher speeds, especially on different terrain types in outdoor applications. Skid-steered vehicles are widely used in robotics, especially for outdoor applications, because of their simple and robust design, high traction and maneuverability. Skid steering is, however, difficult to model, since it is terrain-dependant, and can not be characterized by pure rolling, without slipping and sliding. This makes the path following control of skid-steered vehicles at higher speeds on different terrain types a significant and challenging problem.

In the research community, path following in general is well explored and described. Control of car-like mobile robots is detailed by De Luca et al. in [1]. An example of path following for omnidirectional robots can be found in [2]. Some of the pioneer work on unicycle path following can be found in [3] or [4]. In [5] and [6], examples of model-independent path following control can be found. Williams et al. present a model predictive approach for high speed aggressive driving of a car-like vehicle in [7]. Some work on high speed control on a slippery ground of car-like and double-steering vehicles can be found in [8] or [9]. Soetanto et al. provide a solution for unicycles, and a singularity-free geometric framework for path following in [10]. Indiveri et al. extend this algorithm with additional speed control in [11]. However, none of these approaches explicitly models and controls a skid-steered drive.

Pioneer work on control of wheeled skid-steered vehicles was done by Caracciolo et al. in [12], and further developed by Kozłowski et al. in [13] and [14], Yi et al. in [15] and [16], Lucet et al. in [17], Miller et al. in [18]. However, these algorithms deal with trajectory tracking, and not path following. The advantage of path following over trajectory tracking is clearly stated by Aguiar et al. in [19]. Furthermore, these algorithms are not experimentally evaluated at higher speeds.

Pentzer et al. propose a kinematic mapping in [20], which enables the use of unicycle path following strategies on skid-steered vehicles. They use the controller proposed in [4], and augment the reference path using ICR estimation (see [21]), in order to set an equivalence between unicycle and skid-steered robots. Rajagopalan et al. propose a path following solution for skid-steered vehicles coping with wheel slip in [22], where the maximum speed is $1.0\mathrm{m/s}$ in the real experiments.

Our contributions are as follows:

- We utilize an experimentally verified, terrain-dependent kinematic model proposed in [23] in path coordinates, using the non-singular geometric framework from [10];
- We propose a new nonlinear kinematic controller using the Lyapunov theory, taking the nonholonomic constraint inherent to skid-steered vehicles explicitly into account;
- We propose an additional linear velocity control, based on reachable curvatures and accounting for actuator saturation, inspired by [11];
- We experimentally evaluate the algorithm performance in three different terrain scenarios, at higher speeds (maximum speed reaching $2.5\mathrm{m/s}$), comparing it with two state-of-the-art algorithms, the algorithm proposed in [20], as well as the one proposed in [10], extended with [11].

II. SKID STEERING KINEMATICS

Skid steering models depend on complex interactions between the wheels (or tracks) and the soil. Hence, the kinematic model of skid-steered vehicles needs to have terrain-dependent values, and to implicitly account for dynamic effects to some extent (see [24]). One possibility is to model the kinematics by using the ICR (Instantaneous Centre of Rotation) positions of the vehicle's velocities. This analysis was proposed by Martínez et al. in [25], and further developed by Mandow et al. in [23]. We utilize the model proposed in [23], since it models the sliding velocity to some extent, as well as some mechanical issues. If we observe Fig. 1, we can see that the vehicle's ICR can be expressed in local coordinates as $ICR = (x_{ICR}, y_{ICR})$. The left and the right wheels can be considered as the left and the right tread, having velocities V_l and V_r, respectively. Now it is possible to define $ICR_l = (x_{ICR}, y_{ICRl})$ and $ICR_r =$

Chair of Cognitive Systems, Computer Science Department, University of Tübingen, Sand 1, 72076 Tübingen, Germany {goran.huskic, sebastian.buck, andreas zell}@uni-tuebingen.de

978-1-5090-4633-1/17/$31.00 ©2017 IEEE

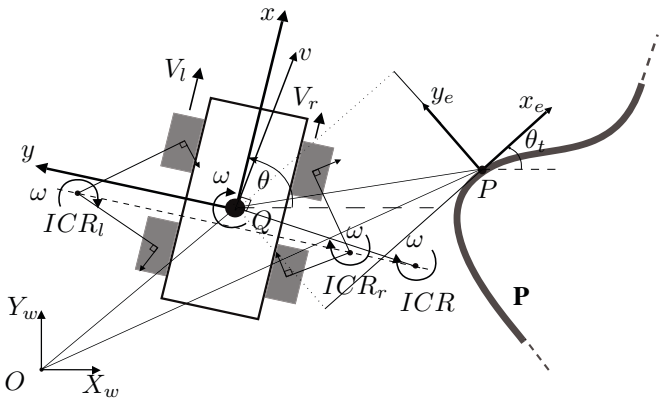

Fig. 1. Path following problem for a skid-steered vehicle.

(x_{ICR}, y_{ICRr}) as the ICR for the left and the right tread, respectively. The angular velocity of each ICR is the same and can be denoted as ω. The vehicle's linear velocity in local coordinates can be expressed as $\boldsymbol{v} = \begin{bmatrix} v_x & v_y \end{bmatrix}^T$. Similar to [23], the kinematic mapping between the velocities of the skid-steered vehicle and its treads can now be expressed in a compact form as

$$\begin{bmatrix} v_x \\ v_y \\ \omega \end{bmatrix} = \frac{1}{y_{ICRr} - y_{ICRl}} \begin{bmatrix} \alpha_l y_{ICRr} & -\alpha_r y_{ICRl} \\ -\alpha_l x_{ICR} & \alpha_r x_{ICR} \\ \alpha_l & -\alpha_r \end{bmatrix} \begin{bmatrix} V_l \\ V_r \end{bmatrix}. \tag{1}$$

Here, α_r and α_l are correction factors that compensate for many mechanical irregularities. Following the work of Caracciolo et al. in [12], the nonholonomic constraint for the skid-steered vehicle can be expressed as

$$x_{ICR}\dot{\theta} + v_y = 0. \tag{2}$$

By integrating this nonholonomic constraint in the vehicle kinematics, as in [13], it is possible to describe the vehicle's motion in global coordinates as

$$\begin{bmatrix} \dot{X} \\ \dot{Y} \\ \dot{\theta} \end{bmatrix} = \begin{bmatrix} \cos\theta & x_{ICR}\sin\theta \\ \sin\theta & -x_{ICR}\cos\theta \\ 0 & 1 \end{bmatrix} \begin{bmatrix} v_x \\ \omega \end{bmatrix}, \tag{3}$$

with $\dot{X}$ and $\dot{Y}$ representing the linear velocity components, and $\dot{\theta}$ representing the angular velocity in the inertial frame, θ being the orientation. The importance of the boundedness of the coordinate x_{ICR} is discussed in [12], [13] and [14]. In these works, the coordinate is forced to be a bounded fixed value. In our work, we experimentally identify the value of x_{ICR} for different terrain types, as well as the rest of the ICR parameters $(y_{ICRl}, y_{ICRr}, \alpha_l, \alpha_r)$.

III. PATH FOLLOWING KINEMATICS

To solve the problem of path following control, it is reasonable to parametrize the kinematic model of the vehicle in path coordinates.

A. Kinematic Model in Path Coordinates

Similar to [10], we define the Serret-Frenet frame as a moving frame $\{F\}$ along the path, as depicted in Fig. 1. The coordinates of this frame are the error coordinates (x_e, y_e). This moving frame $\{F\}$ is sometimes referred to as "the virtual vehicle", a desired configuration which needs to be reached by the actual vehicle.

As presented in Fig. 1, the origin of the frame $\{F\}$ is P, the moving point on the path, which needs to be followed. The point Q is the center of the vehicle. Positions of the points P and Q in the world frame $\{W\}$ can be expressed with vectors $\boldsymbol{p}$ and $\boldsymbol{q}$, respectively. The rotation matrix from $\{F\}$ to $\{W\}$ can be defined as $\boldsymbol{R}(\theta_t)$, where θ_t is the path tangent angle in the point P. The derivative of the angle θ_t can be written as $\dot{\theta}_t = c(s)\dot{s}$, where s is the path curvilinear abscissa, and $c(s)$ is the path curvature parametrized by s. The vector from P to Q can be denoted with $\boldsymbol{r}$, expressed in the frame $\{F\}$. It is now possible to express the velocity of the point Q in global coordinates as

$$\frac{d\boldsymbol{q}}{dt} = \frac{d\boldsymbol{p}}{dt} + \boldsymbol{R}\frac{d\boldsymbol{r}}{dt} + \boldsymbol{R}(\dot{\theta}_t \times \boldsymbol{r}). \tag{4}$$

Using the following expressions

$$\boldsymbol{r} = \begin{bmatrix} x_e \\ y_e \\ 0 \end{bmatrix}, \boldsymbol{q} = \begin{bmatrix} X \\ Y \\ 0 \end{bmatrix}, \boldsymbol{R}^{-1}\frac{d\boldsymbol{p}}{dt} = \begin{bmatrix} \dot{s} \\ 0 \\ 0 \end{bmatrix}, \tag{5}$$

it is possible to write the velocities in error coordinates as

$$\begin{aligned} \dot{x}_e &= \begin{bmatrix} \cos\theta_t & \sin\theta_t \end{bmatrix} \begin{bmatrix} \dot{X} \\ \dot{Y} \end{bmatrix} - \dot{s}(1 - c(s)y_e), \\ \dot{y}_e &= \begin{bmatrix} -\sin\theta_t & \cos\theta_t \end{bmatrix} \begin{bmatrix} \dot{X} \\ \dot{Y} \end{bmatrix} - c(s)\dot{s}x_e. \end{aligned} \tag{6}$$

Now, instead of considering an ideal unicycle, as in [10], we employ a realistic skid steering kinematic model (3). The model of a skid-steered vehicle in (x_e, y_e) coordinates is then

$$\begin{aligned} \dot{x}_e &= v_x\cos\theta_e + x_{ICR}\omega\sin\theta_e - \dot{s}(1 - c(s)y_e), \\ \dot{y}_e &= v_x\sin\theta_e - x_{ICR}\omega\cos\theta_e - c(s)\dot{s}x_e, \\ \dot{\theta}_e &= \omega - c(s)\dot{s}, \end{aligned} \tag{7}$$

where $\theta_e = \theta - \theta_t$.

IV. PATH FOLLOWING CONTROL

Using the previously derived model in path coordinates, it is possible to derive a kinematic control law that drives the errors (x_e, y_e, θ_e) to zero.

A. Kinematic Control in Path Coordinates

We use the following Lyapunov function candidate

$$V_1 = \frac{1}{2}\left(x_e^2 + y_e^2 + \frac{1}{\lambda}|\sin(\theta_e - \delta(y_e, v_x))|\right), \tag{8}$$

where $\delta(y_e, v_x)$ is a function with the property $\delta(0, v_x) = 0$, as proposed in [26]. With the choice of this function, it is possible to shape the transient maneuvers when approaching the path.

The first derivative of the Lyapunov function candidate can be written as

$$\begin{aligned}\dot{V}_1 =& \frac{1}{\lambda}\frac{\sin(\theta_e-\delta)\cos(\theta_e-\delta)}{|\sin(\theta_e-\delta)|}(\dot{\theta}_e-\dot{\delta})+\\ & x_e(v_x\cos\theta_e + x_{ICR}\cos\theta_e + x_{ICR}\omega\sin\theta_e - \dot{s})+\\ & y_e v_x\sin\theta_e - y_e x_{ICR}\omega\cos\theta_e.\end{aligned} \tag{9}$$

Now we define a control law

$$\begin{aligned}\dot{s} &= v_x\cos\theta_e + x_{ICR}\omega\sin\theta_e + k_1 x_e,\\ \dot{\theta}_e &= \dot{\delta} - \frac{|\sin(\theta_e-\delta)|}{\sin(\theta_e-\delta)\cos(\theta_e-\delta)}\Big(-\lambda y_e v_x\sin\theta_e + \\ &\quad \lambda y_e x_{ICR}\omega\cos\theta_e - k_2(\theta_e-\delta)^2\Big),\end{aligned} \tag{10}$$

such that $\dot{V}_1 \leqslant 0$. This algorithm is the proposed kinematic path following control for skid-steered vehicles.

B. System Convergence Analysis

The convergence of the proposed kinematic control law (10) is stated in the following proposition, followed by the proof.

Proposition 1: Let $v_n(t)$ be the desired bounded longitudinal velocity profile applied to the vehicle. If the control law given by (10) is applied to the system given by equations (7), then the errors $x_e(t)$, $y_e(t)$, and $\theta_e(t)$ asymptotically converge to zero, as time t tends to infinity.

Proof: Considering the Lyapunov function candidate V_1 expressed in (8), it is shown that by choosing the control (10), $\dot{V}_1$ becomes negative semi-definite. Thus, V_1 is a positive, monotonically decreasing bounded function. This implies that x_e, y_e and $\theta_e - \delta$ are bounded. Since the lateral velocity $v_y = -x_{ICR}\omega$ is bounded (the parameter x_{ICR} is obtained, such that no excessive skidding appears), v_n and δ are chosen to be bounded, $\dot{\theta}_e$ and $\dot{s}$ are also bounded. Thus, $\dot{x}_e$ and $\dot{y}_e$ are bounded as well. Since $\dot{\delta}$ is bounded as well, it is straightforward to prove that $\ddot{V}_1$ is bounded, and hence $\dot{V}_1$ is uniformly continuous. Following Barbalat's lemma (detailed in e.g. [27]), $\dot{V}_1$ tends to zero, as t tends to infinity. This implies that x_e and $\theta_e - \delta$ tend to zero. It is possible to see that $\ddot{\theta}_e - \ddot{\delta}$ is bounded, such that $\dot{\theta}_e - \dot{\delta}$ is uniformly continuous and tends to zero. Since $\dot{\theta}_e - \dot{\delta}$ tends to zero, x_e needs to tend to zero as well. Then, δ also tends to zero, so θ_e tends to zero as well. Due to the fact that the variables x_e, y_e, and θ_e tend to zero, as t tends to infinity, the robot asymptotically converges to the path. ■

C. Longitudinal Velocity Control

A skid-steered vehicle can drive on paths with almost any curvature. Using the kinematic equations (1), the feasible curvature of a skid-steered vehicle can be expressed as

$$c_r = \frac{\alpha_r V_r - \alpha_l V_l}{\sqrt{(\alpha_r y_{ICRl} V r - \alpha_l y_{ICRr} V_l)^2 + (-\alpha_r x_{ICR} V_r + \alpha_l x_{ICR} V_l)^2}}. \tag{11}$$

This curvature depends on the kinematic parameters, i.e. the ICR centres and correction factors α_r and α_l. Inspired by the work of [11], to avoid turning on the spot while driving, which is especially dangerous at higher speeds, we restrict the wheel velocities to be positive values, limited by a maximum positive value which the actuators provide, i.e. $V_l, V_r \in [0, V_m]$, where V_m is the maximum velocity of a wheel. If we use the relations from the kinematic model (1), and the control law (10), it is possible to express the wheel velocities in the closed loop as

$$\begin{aligned}V_l &= \frac{v_x - y_{ICRl}(\dot{\theta}_e + c_r\dot{s})}{\alpha_l},\\ V_r &= \frac{v_x - y_{ICRr}(\dot{\theta}_e + c_r\dot{s})}{\alpha_r},\end{aligned} \tag{12}$$

and to write the expression for the closed loop curvature

$$c_{cl} = \frac{\dot{\theta}_e + c_r\dot{s}}{\sqrt{v_x^2 + [x_{ICR}(\dot{\theta}_e + c_r\dot{s})]^2}}. \tag{13}$$

Using the expression for the closed loop curvature (13), the maximum velocities for the left and right wheels can be expressed as

$$\begin{aligned}max\{V_l\} &= \frac{v_x + |y_{ICRl}c_{cl}|\sqrt{v_x^2 + [x_{ICR}(\dot{\theta}_e + c_r\dot{s})]}}{\alpha_l},\\ max\{V_r\} &= \frac{v_x + |y_{ICRr}c_{cl}|\sqrt{v_x^2 + [x_{ICR}(\dot{\theta}_e + c_r\dot{s})]}}{\alpha_r}.\end{aligned} \tag{14}$$

Since the control law (10) guarantees that the state variables stay bounded, the closed loop curvature (13) should remain bounded as well. Using the convergence property for the closed loop curvature, we get

$$\lim_{t\to\infty} c_{cl} = \frac{c_r}{\sqrt{1 + (x_{ICR}c_r)^2}}. \tag{15}$$

In (15), x_{ICR} can be considered as a deviation from the closed loop curvature of an ideal differential drive. Using the convergence provided by the control law (10), especially $\lim_{t\to\infty}\dot{\theta}_e = 0$, $\lim_{t\to\infty}\dot{s} = v_x$, and (15), the maximum wheel velocities can be expressed as

$$\begin{aligned}max\{V_l\} &= \frac{v_x(1 + |y_{ICRl}c_r|)}{\alpha_l},\\ max\{V_r\} &= \frac{v_x(1 + |y_{ICRr}c_r|)}{\alpha_r},\end{aligned} \tag{16}$$

when $t \to \infty$. If the maximum actuator speeds of the left and the right wheel are the same, it can be written that $max\{V_l\} = max\{V_r\} = V_m$. The linear velocity of skid-steered vehicles behaves asymmetrically, and should accordingly be adjusted, also considering the actuator saturation.

We propose the following longitudinal velocity control, in order to cope with the asymmetrical behaviour of skid-steered vehicles

$$\begin{aligned}{}^{\omega\geqslant 0}v_x &= \begin{cases}\frac{-\alpha_r y_{ICRl}V_m}{y_{ICRr} - y_{ICRl}}, & V_1 \geqslant \epsilon.\\ \frac{\alpha_r V_m}{1+|y_{ICRr}c_r|}, & V_1 < \epsilon.\end{cases}\\ {}^{\omega<0}v_x &= \begin{cases}\frac{\alpha_l y_{ICRr}V_m}{y_{ICRr} - y_{ICRl}}, & V_1 \geqslant \epsilon.\\ \frac{\alpha_l V_m}{1+|y_{ICRl}c_r|}, & V_1 < \epsilon.\end{cases}\end{aligned} \tag{17}$$

Here, ϵ is a free positive parameter. The idea behind this, similar to [11], is to allow greater longitudinal velocities only when the path following error is small enough and the convergence provided by the control algorithm (10) can be used. This path following error is measured by the Lyapunov function V_1. If the error is small enough, the longitudinal velocity is computed using (16), and the computation is depending on the turning direction, i.e. whether the right or the left tread is dominant. If the error is above the properly chosen threshold ϵ, the longitudinal velocity v_x is computed using (1), also depending on the turning direction.

V. EXPERIMENTAL RESULTS

The proposed algorithm is implemented in the ROS (Robot Operating System) framework (more details in [28]), and tested on a Summit XL mobile robot from the company Robotnik (see Fig. 2), together with the algorithm proposed in [20], and the one proposed in [10], extended with [11]. To simplify the notation, the algorithm proposed in [20]

Fig. 2. Skid-steered robot used in the experiments: Summit XL.

is referred to as PBR, and the one from [10] and [11] as SLPINL, using the surname initials of the authors involved. These two algorithms, together with the proposed one, were tested on three different terrain types: grass, vinyl and macadam (crushed stones mixed with fine dust and sand), which can be seen in Fig. 3. The ICR parameters

(a) grass (b) vinyl (c) macadam

Fig. 3. Three different terrain types used for the experiments: grass, vinyl and macadam.

are estimated for the three different terrain types similar to [23], using evolutionary algorithms and two software tools developed at our department (see [29], and [30]).

In all experiments, PBR and SLPINL were commanded with same desired velocities, to achieve similar average velocities, and the proposed approach was commanded with even higher velocities, to demonstrate its advantages.

A. Grass

For the experiments on grass, a 159.83m long path was planned, with representative curvatures and straight line segments. As the ground truth, a fusion of odometry from Hall effect sensors, and an internal gyroscope was used, which is the default odometric system of Summit XL robots, providing the pose at $50Hz$. The localization error was measured using CS::APEX (described in [30]), and at the average speed of 0.89m/s the error was $x = 0.015\text{m}$, $y = 0.69\text{m}$, $\theta = 2.94°$, while at 2.15m/s it was $x = 0.62\text{m}$, $y = -0.65\text{m}$, $\theta = 3.85°$. The results of path following experiments at different velocities can be seen in Fig. 4. While all of the three algorithms perform very well up to

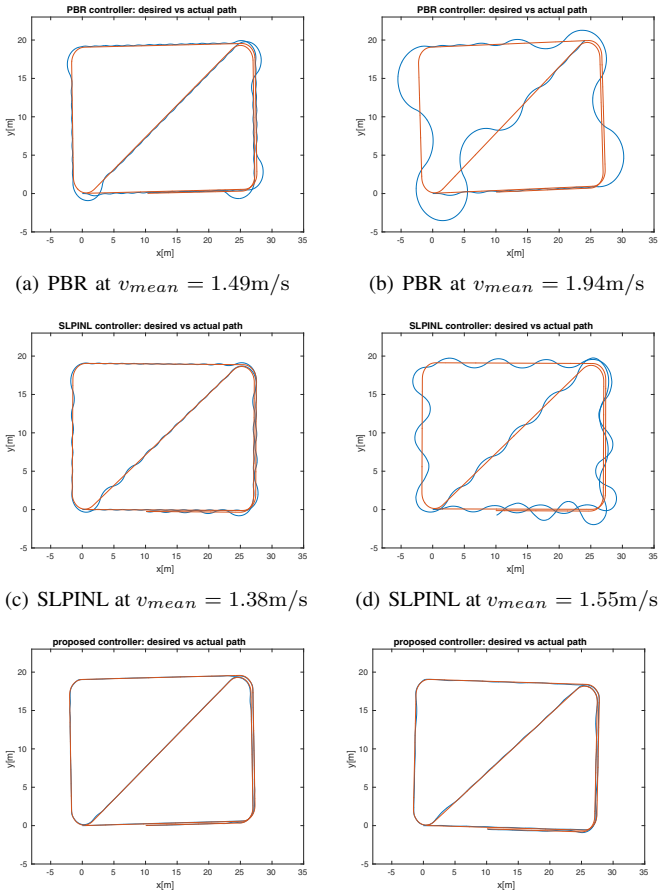

(a) PBR at $v_{mean} = 1.49\text{m/s}$ (b) PBR at $v_{mean} = 1.94\text{m/s}$

(c) SLPINL at $v_{mean} = 1.38\text{m/s}$ (d) SLPINL at $v_{mean} = 1.55\text{m/s}$

(e) The proposed approach at $v_{mean} = 1.73\text{m/s}$ (f) The proposed approach at $v_{mean} = 2.15\text{m/s}$

Fig. 4. Experiments on grass, following a 159.83m long path (red line - desired, blue line - actual).

1.0m/s, at around 1.5m/s PBR has an increased error in the curves, and SLPINL reaches oscillating behaviour. At around 2m/s SLPINL isn't able to keep the robot on the path, and PBR enters oscillations, with a maximum error of 3.61m. At the average speed of 1.73m/s, the proposed algorithm has a maximum error of 16cm, and an average error of 3.3cm. At the average speed of 2.15m/s, the maximum error is 22.36cm, the mean error 6.9cm, and the maximum speed is 2.54m/s. The relation between the average speed and the average error for these experiments is visualized in Fig. 5.

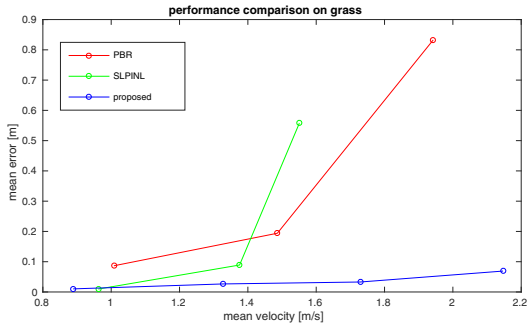

Fig. 5. Performance comparison on grass: two state-of-the-art algorithms and the proposed one

B. Vinyl

For the indoor experiments conducted in a corridor, on a vinyl floor, a Bernoulli lemniscate was chosen as a desired path, because of its challenging curvature. The goal was to follow five overlayed lemniscates, to demonstrate the repeatability. The total length of the desired path was 110.77m, and the results of path following can be seen in Fig. 6. The robot was localized using a Velodyne VLP-16 3D laser scanner, and 3 special pillars as landmarks. Using odometry and triangulated laser measurements as inputs for an Extended Kalman Filter, the robot's pose was available at $10Hz$. This localization system was implemented using CS::APEX ([30]). The PBR algorithm has a mean error of 14.5cm while driving with an average speed of 1.01m/s. At higher speeds, the maximum error rises over 1m, and the following task cannot be executed in a narrow corridor. The SLPINL algorithm has a mean error of only 4.2cm at 0.87m/s, but already at 1.05m/s, the maximum error reaches values higher than 1m.

Using the proposed algorithm at 1.34m/s, the mean error is 4.6cm, while at 1.64m/s the mean error is 8.5cm. To show the robustness of the algorithm, the experiments with the proposed approach are also conducted using different values of the kinematic ICR parameters. At the average velocity of 1.4m/s, when using macadam parameters on vinyl, the mean error is 4.6cm, and when using grass parameters on vinyl, the mean error is 4.9cm. This shows a high robustness of the algorithm to parameter changes.

C. Macadam

For the outdoor experiments conducted on macadam, the same desired path and localization system were used, as in the case of the experiments on vinyl. In Fig. 7 the results of path following on macadam are presented. At 1m/s, the PBR controller gives a mean error of 16.3cm, while at 1.48m/s the mean error is 85.6cm, and the maximum error is 2.12m. The SLPINL controller gives a mean error of 7.3cm at 0.87m/s, while at 0.94m/s, the following control task cannot be executed. The proposed approach has a mean error of 5.2cm at 1.1m/s, while at 1.68m/s, the mean error is 18.3cm. In Fig. 7(e), a localization error as a sudden jump of 88.6cm can be seen. The controller is still able to keep the track of the path, which demonstrates the robustness of the approach to localization errors.

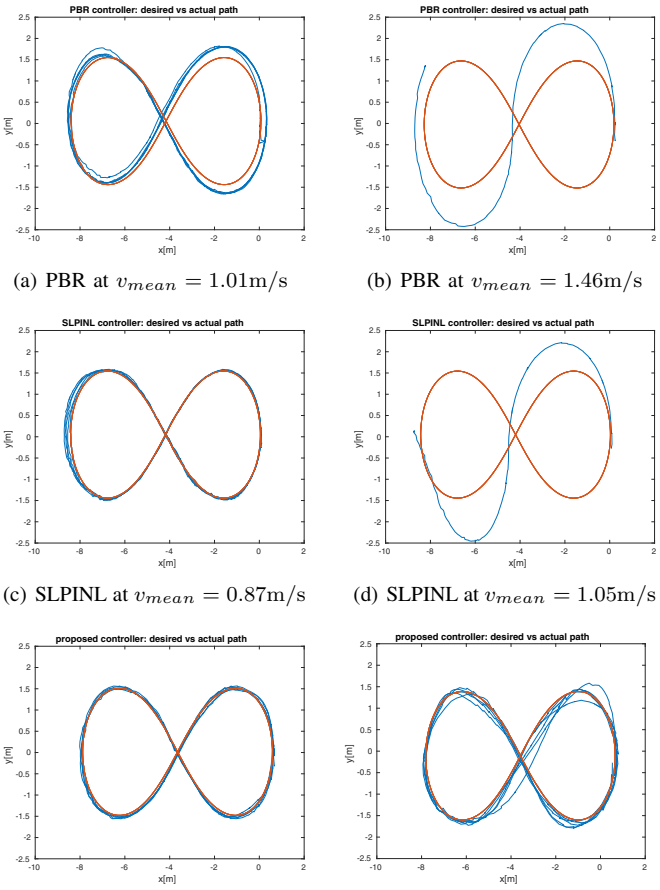

(a) PBR at $v_{mean} = 1.01\text{m/s}$ (b) PBR at $v_{mean} = 1.46\text{m/s}$

(c) SLPINL at $v_{mean} = 0.87\text{m/s}$ (d) SLPINL at $v_{mean} = 1.05\text{m/s}$

(e) The proposed approach at $v_{mean} = 1.34\text{m/s}$ (f) The proposed approach at $v_{mean} = 1.64\text{m/s}$

Fig. 6. Experiments on vinyl, following a 110.77m long path (red line - desired, blue line - actual).

VI. CONCLUSIONS

We propose a new nonlinear control law for the path following task of skid-steered mobile robots at higher speeds on different terrain types. Convergence of the robot to the path is formally proven. In the experimental evaluation [1], where three different terrain scenarios are used, the proposed algorithm outperforms two state-of-the-art algorithms. Using the proposed algorithm, the robot is able to follow challenging paths, on different, challenging terrain types, at higher speeds. The control performance is demonstrated to be robust to parameter changes, as well as to localization errors.

Future work includes utilizing a dynamic model of skid-steered vehicles, as well as detecting the wheel slip.

ACKNOWLEDGEMENTS

This work was partially developed during the participation in the robotics competition SpaceBot Camp 2015, organized by the German Aerospace Center (DLR).

Goran Huskić would like to thank the German Academic Exchange Service (DAAD) for his Ph.D. scholarship.

[1] A video demonstrating the proposed algorithm's performance can be found at `https://youtu.be/plaoHHEfM3o` .

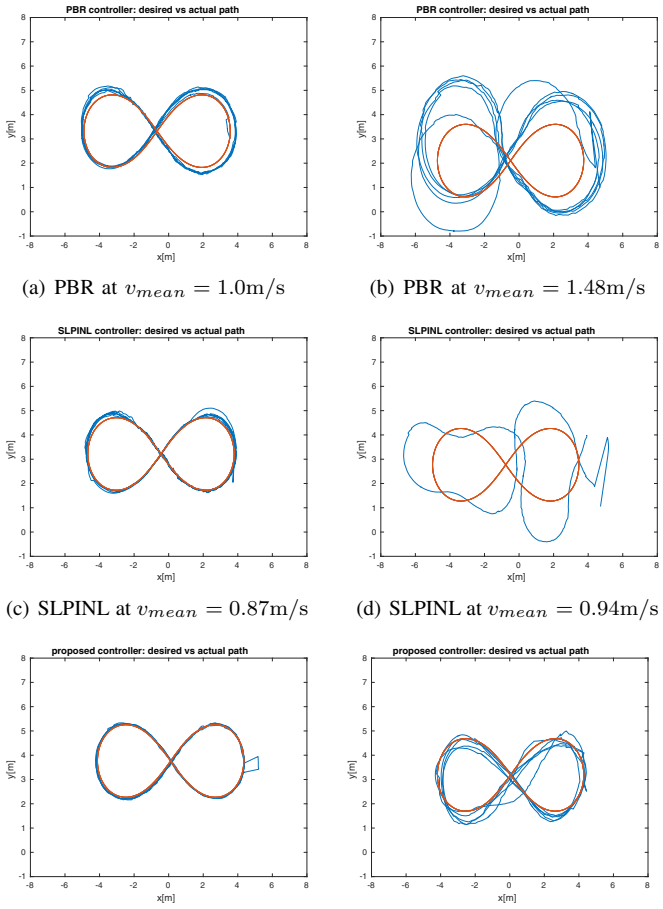

(a) PBR at $v_{mean} = 1.0\text{m/s}$ (b) PBR at $v_{mean} = 1.48\text{m/s}$

(c) SLPINL at $v_{mean} = 0.87\text{m/s}$ (d) SLPINL at $v_{mean} = 0.94\text{m/s}$

(e) The proposed approach at $v_{mean} = 1.1\text{m/s}$ (f) The proposed approach at $v_{mean} = 1.68\text{m/s}$

Fig. 7. Experiments on macadam, following a 110.77m long path (red line - desired, blue line - actual).

REFERENCES

[1] A. De Luca, G. Oriolo, and C. Samson, "Feedback control of a nonholonomic car-like robot," in *Robot motion planning and control*. Springer, 1998, pp. 171–253.

[2] K. Kanjanawanishkul and A. Zell, "Path following for an omnidirectional mobile robot based on model predictive control," in *Robotics and Automation, 2009. ICRA'09. IEEE International Conference on*. IEEE, 2009, pp. 3341–3346.

[3] C. Samson, "Path following and time-varying feedback stabilization of a wheeled mobile robot," in *Int. Conf. ICARCV'92*, 1992.

[4] C. C. de Wit, H. Khennouf, C. Samson, and O. Sordalen, "Nonlinear control design for mobile robots," in *Recent Developments in Mobile Robots*. World Scientific, 1993.

[5] R. Oftadeh, R. Ghabcheloo, and J. Mattila, "A time-optimal bounded velocity path-following controller for generic wheeled mobile robots," in *Robotics and Automation (ICRA), 2015 IEEE International Conference on*. IEEE, 2015, pp. 676–683.

[6] G. Huskić, S. Buck, and A. Zell, "A simple and effcient path following algorithm for wheeled mobile robots," in *Intelligent Autonomous Systems (IAS-14)*. Springer, 2016.

[7] G. Williams, P. Drews, B. Goldfain, J. M. Rehg, and E. A. Theodorou, "Aggressive driving with model predictive path integral control," in *2016 IEEE International Conference on Robotics and Automation (ICRA)*. IEEE, 2016, pp. 1433–1440.

[8] R. Lenain, B. Thuilot, C. Cariou, and P. Martinet, "High accuracy path tracking for vehicles in presence of sliding: Application to farm vehicle automatic guidance for agricultural tasks," *Autonomous robots*, vol. 21, no. 1, pp. 79–97, 2006.

[9] E. Lucet, R. Lenain, and C. Grand, "Dynamic path tracking control of a vehicle on slippery terrain," *Control Engineering Practice*, vol. 42, pp. 60–73, 2015.

[10] D. Soetanto, L. Lapierre, and A. Pascoal, "Adaptive, non-singular path-following control of dynamic wheeled robots," in *Decision and Control, 2003. Proceedings. 42nd IEEE Conference on*, vol. 2. IEEE, 2003, pp. 1765–1770.

[11] G. Indiveri, A. Nüchter, and K. Lingemann, "High speed differential drive mobile robot path following control with bounded wheel speed commands," in *Robotics and Automation, 2007 IEEE International Conference on*. IEEE, 2007, pp. 2202–2207.

[12] L. Caracciolo, A. De Luca, and S. Iannitti, "Trajectory tracking control of a four-wheel differentially driven mobile robot," in *Robotics and Automation, 1999. Proceedings. 1999 IEEE International Conference on*, vol. 4. IEEE, 1999, pp. 2632–2638.

[13] K. Kozłowski and D. Pazderski, "Modeling and control of a 4-wheel skid-steering mobile robot," *Int. J. Appl. Math. Comput. Sci*, vol. 14, no. 4, pp. 477–496, 2004.

[14] K. Kozlowski and D. Pazderski, "Practical stabilization of a skid-steering mobile robot-a kinematic-based approach," in *Proc. IEEE 3rd Int. Conf. on Mechatronics*, 2006, pp. 519–524.

[15] J. Yi, D. Song, J. Zhang, and Z. Goodwin, "Adaptive trajectory tracking control of skid-steered mobile robots," in *Robotics and Automation, 2007 IEEE International Conference on*. IEEE, 2007, pp. 2605–2610.

[16] J. Yi, H. Wang, J. Zhang, D. Song, S. Jayasuriya, and J. Liu, "Kinematic modeling and analysis of skid-steered mobile robots with applications to low-cost inertial-measurement-unit-based motion estimation," *Robotics, IEEE Transactions on*, vol. 25, no. 5, pp. 1087–1097, 2009.

[17] E. Lucet, C. Grand, D. Sallé, and P. Bidaud, "Dynamic velocity and yaw-rate control of the 6wd skid-steering mobile robot roburoc6 using sliding mode technique," in *IEEE/RSJ International Conference on Intelligent Robots and Systems, St. Louis, Missouri, USA*, 2009.

[18] L. M. Miller and T. D. Murphey, "Simultaneous optimal parameter and mode transition time estimation," in *Intelligent Robots and Systems (IROS), 2012 IEEE/RSJ International Conference on*. IEEE, 2012, pp. 719–724.

[19] A. P. Aguiar, D. B. Dačić, J. P. Hespanha, and P. Kokotović, "Path-following or reference-tracking?" *rn*, vol. 1, p. 1, 2004.

[20] J. Pentzer, S. Brennan, and K. Reichard, "The use of unicycle robot control strategies for skid-steer robots through the icr kinematic mapping," in *Intelligent Robots and Systems (IROS 2014), 2014 IEEE/RSJ International Conference on*. IEEE, 2014, pp. 3201–3206.

[21] ——, "Model-based prediction of skid-steer robot kinematics using online estimation of track instantaneous centers of rotation," *Journal of Field Robotics*, vol. 31, no. 3, pp. 455–476, 2014.

[22] V. Rajagopalan, A. Kelly, *et al.*, "Slip-aware model predictive optimal control for path following," in *2016 IEEE International Conference on Robotics and Automation (ICRA)*. IEEE, 2016, pp. 4585–4590.

[23] A. Mandow, J. L. Martinez, J. Morales, J. L. Blanco, A. Garcia-Cerezo, and J. Gonzalez, "Experimental kinematics for wheeled skid-steer mobile robots," in *Intelligent Robots and Systems, 2007. IROS 2007. IEEE/RSJ International Conference on*. IEEE, 2007, pp. 1222–1227.

[24] J. Y. Wong, *Theory of ground vehicles*. John Wiley & Sons, 2001.

[25] J. L. Martínez, A. Mandow, J. Morales, S. Pedraza, and A. García-Cerezo, "Approximating kinematics for tracked mobile robots," *The International Journal of Robotics Research*, vol. 24, no. 10, pp. 867–878, 2005.

[26] A. Micaelli and C. Samson, "Trajectory tracking for unicycle-type and two-steering-wheels mobile robots," 1993.

[27] H. K. Khalil and J. Grizzle, *Nonlinear systems*. Prentice hall New Jersey, 1996, vol. 3.

[28] M. Quigley, K. Conley, B. Gerkey, J. Faust, T. Foote, J. Leibs, R. Wheeler, and A. Y. Ng, "Ros: an open-source robot operating system," in *ICRA workshop on open source software*, vol. 3, no. 3.2, 2009, p. 5.

[29] M. Kronfeld, H. Planatscher, and A. Zell, "The eva2 optimization framework," in *International Conference on Learning and Intelligent Optimization*. Springer, 2010, pp. 247–250.

[30] S. Buck, R. Hanten, C. R. Pech, and A. Zell, "Synchronous dataflow and visual programming for prototyping robotic algorithms," in *Intelligent Autonomous Systems (IAS-14)*. Springer, 2016.